MOX-Report No. 14/2017

Finite Element approximation of an evolutionary Topology Optimization problem

Bruggi, M.; Parolini, N.; Regazzoni, F.; Verani, M.

MOX, Dipartimento di Matematica
Politecnico di Milano, Via Bonardi 9 - 20133 Milano (Italy)

mox-dmat@polimi.it http://mox.polimi.it

Finite Element approximation of an evolutionary Topology Optimization problem

Matteo Bruggi[♯], Nicola Parolini[♭], Francesco Regazzoni[♭] and Marco Verani[♭]

February 23, 2017

[♯] Dipartimento di Ingegneria Civile e Ambientale,
Politecnico di Milano
Piazza Leonardo da Vinci 32, 20133 Milano, Italy

matteo.bruggi@polimi.it

[♭] MOX - Dipartimento di Matematica,
Politecnico di Milano
Piazza Leonardo da Vinci 32, 20133 Milano, Italy

nicola.parolini@polimi.it, francesco.regazzoni@polimi.it, marco.verani@polimi.it

Abstract

We present a topology optimization based procedure aiming at the optimal placement (and design) of the supports in problems characterized by a time dependent construction process. More precisely, we focus on the solution of a time-dependent minimal compliance problem based on the classical *Solid Isotropic Material with Penalization* (SIMP) method. In particular, a continuous optimization problem with the state equation defined as the time-integral of a linear elasticity problem on a space-time domain is firstly introduced and the mean compliance over a time interval objective functional is then selected as objective function. The optimality conditions are derived and a fixed-point algorithm is introduced for the iterative computation of the optimal solution. Numerical examples showing the differences between a standard SIMP method, which only optimizes the shape at the final time, and the proposed time-dependent approach are presented and discussed.

1 Introduction

Topology optimization is a powerful design tool that is extensively adopted in many branches of engineering to find optimal layouts that maximize target performances, see [2, 11, 5]. The conventional approach searches for the distribution of a prescribed amount of isotropic material such that the so–called compliance (twice the elastic strain energy computed at equilibrium) is minimized. A suitable interpolation can be adopted to penalize the mechanical properties of the elastic body depending on the local values of the unknown density field. In most cases, 0–1 solutions can be straightforwardly found implementing the well–known SIMP (Solid Isotropic Material with Penalization) [1]. Different methods are available in the literature to solve the so–called volume-constrained minimum compliance problem: among the others, one can use Optimality Criteria, see, e.g., [9] or methods of sequential convex

programming such as CONLIN [6] and MMA [12]. All the above iterative approaches generally resort to the adoption of the finite element method to solve the equilibrium equation and compute the objective function and its sensitivity with respect to the design variables.

In general, most of the approaches for topology optimization deals with loads that are time–independent, with the main goal of optimizing a structure for an assigned set of constraints/supports. The work in [4] firstly introduced a design formulation attacking simultaneously the structural topology and the constraint locations, introducing new variables and enforcing a prescribed amount of allowable support. Afterwards, the work by [15] introduced a two–step procedure for the integrated layout design of supports and structures. Supports are intended as components that are partially embedded into the design domain and subjected to the applied boundary conditions. First, the optimal position of movable support components is found along a prescribed boundary of the design domain, then the layout optimization of the support components and the structure is performed. Both approaches cope with time–independent loads.

Several formulations exist to cope with the dynamic compliance of structures, see e.g. [8, 7] and [13] but, to the authors' knowledge, no numerical method has been investigated yet to cope with the optimal design of supports in problems involving time dependent construction stages. For the sake of exposition, let us consider a specimen with a prescribed shape that is manufactured through a sequence of construction steps requiring the adoption of a suitable set of supports. The self–weight of the specimen is the prevalent design load that, in turn, depends itself on the evolution in time of the construction process. Hence, the bearing elements should be optimized to provide the stiffest support *throughout* the stages. This means that the compliance–based objective function should account not only for the final configuration, but also for *all* the intermediate shapes that are handled during the construction.

The need for the solution of the outlined design problem arises in many fields of applications, see, e.g., the construction of a bridge or the distribution of supports to perform 3D printing of complex shapes. Additive manufacturing, also known as 3D printing, nowadays is extensively used to create prototypes from digital models. Successive layers of material are laid down by a three–dimensional printer requiring support structures to sustain overhanging surfaces. Up to now, not any shape or geometry can be printed in real time, because a suitable set of supports must be engineered before synthesizing the three–dimensional object. Support structures remarkably affect not only the processing times but also the material consumption so their rationale design is crucial to improve the overall process of 3D printing. It must be finally remarked that additive manufacturing itself is a fertile area of research for topology optimization. In fact, 3D printing fills the gap between topology optimization and application, since any computed optimal design can be printed with minimal limitations on its complexity, see [14].

Goal of this work is to propose a new approach for the optimal placement (and design) of the supports in problems involving construction stages, thus including the inherent time–dependent nature of the process.

To this aim, a continuous optimization problem adopting a state equation defined as the time–integral of a linear elasticity problem on a space–time domain is formulated, while the objective function is given by the time-averaged compliance. The optimality conditions for this optimization problem are derived and a fixed-point algorithm is introduced for the iterative computation of the optimal solution. The equivalence between the *integral-in-time* formulation, used for the theoretical derivation of the optimality conditions, and a *pointwise-*

in-time formulation of the state equation, exploited in the numerical approximation, is shown. The discretization of the optimization problem is finally obtained by considering n intermediate time instants t_i (and the corresponding spatial domains $\Omega(t_i)$) and solving a sequence of linear elasticity problems on $\Omega(t_i)$ with the finite element method. Numerical simulations obtained with this evolutionary topology optimization procedure have been firstly announced in [3], while in the present work we supply the theoretical framework in which the evolutionary continuous problem is defined as well as a detailed derivation of the resulting numerical scheme.

The outline of the paper is as follows. Sections 2 and 3 define the continuous and discrete topology optimization problems with the aim of designing the supports of an object exhibiting the minimum mean compliance over a time interval. Section 4 provides numerical examples showing the differences between a conventional SIMP method, which only optimizes the shape at the final time, and the proposed time–dependent approach. Section 5 provides final remarks on the presented methodology.

2 The continuous evolutionary topology optimization problem

In this section we describe the topology optimization problem which will be instrumental to optimally place the supports of the target object to be printed.

2.1 Preliminaries

Let us consider an hold-all cylindrical space domain $\Omega = E \times (0,h) \subset \mathbb{R}^{d-1} \times \mathbb{R}^+$, with $d = 2,3$ and E a subset of $\mathbb{R}^{d-1}$. Each point in Ω reads as $\mathbf{x} = (\mathbf{x}^*, y)$, where $\mathbf{x}^*$ denotes the planar component while y is the vertical one. Once the printing process is complete, i.e. for $t = T$, the target object $\mathcal{O}$ will occupy a certain subset $\Omega_1 \subset \Omega$, while for $t < T$ it will occupy intermediate configurations $\Omega_1(t)$ such that $\Omega_1(t) \subset \Omega$. In view of the above discussion, the value h represents the height of the object at the final time T. For future use, we also introduce the subdomain $\Omega_0 \subset \Omega$ identifying the region where *a priori* the user does not want to introduce any support. Next, we introduce a time-dependent domain $\Omega(t)$ that changes during the additive manufacturing process and represents the region where the 3D printer can add material (either belonging to the object or to the supports). We assume that $\Omega(t)$ grows in the direction given by the coordinate y with constant velocity v_0, i.e. $\Omega(t) = \{(\mathbf{x}^*, y) \in E \times (0,h) : 0 < y < v_0 t\}$. Accordingly, we have $\Omega_1(t) = \Omega(t) \cap \Omega_1$ (see Figure 1). Clearly, at the final time $T = h/v_0$, we have $\Omega(T) = \Omega$ and $\Omega_1(T) = \Omega_1$.

In order to set up the topology optimization problem, we need to introduce a proper space-time domain and a suitable functional space. First, we define a proper space-time domain Q_T which is only a subset of $\Omega \times [0,T]$. This is motivated by the fact that at each time t we do not want to consider the whole Ω, but just a subset $\Omega(t)$. In view of this, we set (see Figure 2)

$$Q_T = \cup_{t\in[0,T]} \big\{(\mathbf{x},t) : \mathbf{x} \in \Omega(t)\big\}. \tag{2.1}$$

Then we introduce the functional space $\tilde{\mathcal{V}}$ whose members are collections of displacement fields, one for each time in $[0,T]$. Let $\Gamma_D \subset \partial\Omega$ be the portion of the boundary where the

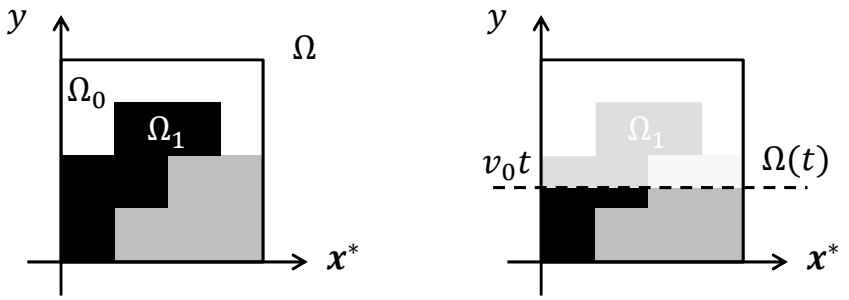

Figure 1: a) Reference space domain. b) Space domain relative to time t. $\Omega(t)$ is located below the dotted line, corresponding to the height $v_0 t$).

object is anchored. In the following we assume for simplicity that Γ_D is a subset of the lower boundary $E \times \{0\}$. The functional space $\tilde{\mathcal{V}}$ reads as follows

$$\tilde{\mathcal{V}} = \Big\{ \mathbf{u} : Q_T \to \mathbb{R}^d \text{ s.t. } \mathbf{u}(\mathbf{x}, s) \in H^1_{0,\Gamma_D}(\Omega(s)) \quad \text{for a.e. } s \in [0,T], \\ \int_0^T \big\| \mathbf{u}(\mathbf{x}, s) \big\|^2_{H^1_{0,\Gamma_D}(\Omega(s))} \, \mathrm{d}s < +\infty \Big\}. \tag{2.2}$$

In the sequel we will denote by $\mathbf{u}(s) := \mathbf{u}(\mathbf{x}, s)$ the displacement field at time s. Finally, we define $\mathcal{V}$ as the quotient set of $\tilde{\mathcal{V}}$ with respect to almost everywhere equivalence. The following result shows that $\mathcal{V}$ is an Hilbert space when endowed with a proper scalar product.

Proposition 1. *$\mathcal{V}$ is an Hilbert space endowed with the scalar product*

$$\big(\mathbf{u}, \mathbf{v}\big)_{\mathcal{V}} = \int_0^T \int_{\Omega(t)} \nabla \mathbf{u}(t) : \nabla \mathbf{v}(t) \, \mathrm{d}\mathbf{x} \, \mathrm{d}t. \tag{2.3}$$

Proof. Since it can be easily proved that $(\cdot, \cdot)_{\mathcal{V}}$ is a scalar product, in the sequel we just show the completeness. Let $\{\mathbf{u}_j\}_{j \geq 1} \in \mathcal{V}$ be a Cauchy sequence such that (possibly passing to subsequences and with an abuse of notation) there holds

$$\|\mathbf{u}_{j+1} - \mathbf{u}_j\|_{\mathcal{V}} \leq \frac{1}{2^j} \quad \forall j \geq 1. \tag{2.4}$$

In the following we prove that $\{\mathbf{u}_j\}$ is convergent in $\mathcal{V}$. For $t \in [0,T]$ let us introduce the sequence $\{g_n(t)\}_{n \geq 1}$ with

$$g_n(t) = \sum_{j=1}^{n} \|\mathbf{u}_{j+1}(t) - \mathbf{u}_j(t)\|_{H^1_0(\Omega(t))}.$$

It is immediate to verify that the sequence g_n is monotone increasing and $\|g_n\|_{L^2(0,T)} \leq C$ for every n, where the constant C is independent of t. Employing the Monotone Convergence

Theorem we get that the sequence $g_n(t)$ pointwise converges to a finite limit $g(t)$ a.e. in the time interval. Moreover, it holds

$$\|g\|_{L^2(0,T)} \leq \|g_n - g\|_{L^2(0,T)} + \|g_n\|_{L^2(0,T)} < +\infty. \tag{2.5}$$

On the other hand, by using the triangle inequality, for $m \geq n \geq 2$ we have a.e. in the time interval.

$$\begin{aligned} \|\mathbf{u}_m(t) - \mathbf{u}_n(t)\|_{H_0^1(\Omega(t))} &\leq \|\mathbf{u}_m(t) - \mathbf{u}_{m-1}(t)\|_{H_0^1(\Omega(t))} + \ldots + \|\mathbf{u}_{n+1}(t) - \mathbf{u}_n(t)\|_{H_0^1(\Omega(t))} \\ &\leq g(t) - g_{n-1}(t). \end{aligned}$$

Hence, $\{\mathbf{u}_j(t)\}_{j\geq 1}$ is a Cauchy sequence in $H_0^1(\Omega(t))$. As this latter space is complete, there exists $\mathbf{u}(t)$ such that

$$\|\mathbf{u}_j(t) - \mathbf{u}(t)\|_{H_0^1(\Omega(t))} \to 0 \quad \text{for } j \to +\infty, \tag{2.6}$$

a.e in time. Moreover, employing the triangle inequality together with (2.5) and the fact that $u_1 \in \mathcal{V}$ we have for $j \geq 1$

$$\begin{aligned} \|\mathbf{u}_j(t)\|_{H_0^1(\Omega(t))} &\leq \sum_{k=1}^{j-1} \|\mathbf{u}_{k+1}(t) - \mathbf{u}_k(t)\|_{H_0^1(\Omega(t))} + \|\mathbf{u}_1(t)\|_{H_0^1(\Omega(t))} \\ &\leq g(t) + \|\mathbf{u}_1(t)\|_{H_0^1(\Omega(t))} \in L^2(0,T). \end{aligned} \tag{2.7}$$

Finally, combining (2.6)-(2.7) with the Dominated Convergence Theorem we conclude that

$$\|\mathbf{u}_j - \mathbf{u}\|_{\mathcal{V}} \to 0 \quad \text{for } j \to +\infty,$$

i.e. $\mathbf{u}_j \to \mathbf{u}$ in $\mathcal{V}$.

□

2.2 Design space

In this section we introduce the design variable which describes the material distribution. As it is common in topology optimization, it is introduced as a non-dimensional density distribution ρ. More specifically, in our framework we define the set of admissible densities as follows

$$\begin{aligned} \mathcal{U}_{ad} = \Big\{ \rho(\mathbf{x}) \in L^2(\Omega) \,:\, & \rho \geq \rho_{min} && \text{a.e. in } \Omega, && \text{(2.8a)} \\ & \rho \leq 1 && \text{a.e. in } \Omega, && \text{(2.8b)} \\ & \rho = \rho_{min} && \text{a.e. in } \Omega_0, && \text{(2.8c)} \\ & \rho = 1 && \text{a.e. in } \Omega_1, && \text{(2.8d)} \\ & \int_\Omega \rho \, \mathrm{d}\mathbf{x} \leq C \Big\} && && \text{(2.8e)} \end{aligned}$$

Proposition 2. *$\mathcal{U}_{ad}$ is a closed and convex set.*

Proof. Let $\{\rho_n\}_n$ be a sequence in $\mathcal{U}_{ad}$, such that $\rho_n \to \rho$ in $L^2(\Omega)$. It exists a subsequence $\{\rho_{n_k}\}_k$ such that $\rho_{n_k} \to \rho$ a.e., and so (2.8a)-(2.8d) are satisfied by the limit. Since $L^2(\Omega) \hookrightarrow L^1(\Omega)$, then $\rho_n \to \rho$ in $L^1(\Omega)$ and so $\int_\Omega \rho \, \mathrm{d}\mathbf{x} \leq C$. Thus $\mathcal{U}_{ad}$ is closed. Convexity is trivial to be proved. □

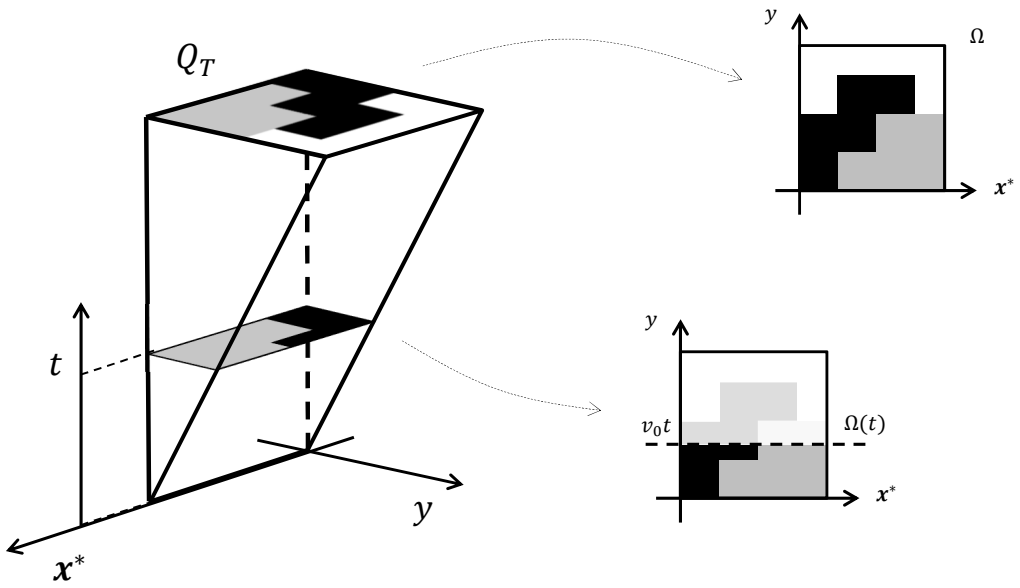

Figure 2: Space-time domain Q_T.

2.3 State Equation

We require that at each time t, the state variable $\mathbf{u}(t)$ has to satisfy a linear elasticity problem on $\Omega(t)$. We define a bilinear form associated to time t as follows:

$$a_\rho(\mathbf{u}, \mathbf{v}; t) = \int_{\Omega(t)} \mathbf{E}(\rho(\mathbf{x})) \nabla_s \mathbf{u}(t) : \nabla_s \mathbf{v}(t) \, \mathrm{d}\mathbf{x} \tag{2.9}$$

where $\mathbf{E}(\rho(\mathbf{x})) = E_\rho(\mathbf{x})\mathbf{E}_0$, being $\mathbf{E}_0$ the elasticity tensor of the considered material, and $E_\rho(\mathbf{x})$ is the dimensionless Young modulus, given by the SIMP interpolation, i.e.

$$E_\rho(\mathbf{x}) = E_{min} + \rho(\mathbf{x})^p (1 - E_{min}). \tag{2.10}$$

We introduce the following pointwise-in-time problem: find $\mathbf{u} \in \mathcal{V}$ such that

$$a_\rho(\mathbf{u}, \mathbf{v}; t) = l(\mathbf{v}; t) \qquad \forall \, \mathbf{v} \in H^1_{0,\Gamma_D}(\Omega) \quad \text{a.e. } t \in [0, T], \tag{2.11}$$

where $l(\mathbf{v}; t)$ is the continuous functional on $H^1_{\Gamma_D}(\Omega(t))$ representing the external load at time t associated with the weight of the target object. In view of this, the functional $l(\mathbf{v}; t)$ is defined as:

$$l(\mathbf{v}; t) = \int_{\Omega_1(t)} \rho_0 \mathbf{g} \cdot \mathbf{v} \, \mathrm{d}\mathbf{x}, \tag{2.12}$$

being ρ_0 the density of the material used by the printer and $\mathbf{g}$ the gravity force.

We now show that the pointwise-in-time problem (2.11) is equivalent to the following "averaged" problem: find $\mathbf{u} \in \mathcal{V}$ such that

$$\bar{a}_\rho(\mathbf{u}, \mathbf{v}) = \bar{l}(\mathbf{v}) \quad \forall \mathbf{v} \in \mathcal{V}, \tag{2.13}$$

where we define:

$$\bar{a}_\rho(\mathbf{u},\mathbf{v}) = \frac{1}{T}\int_0^T a_\rho(\mathbf{u},\mathbf{v};t)\,\mathrm{d}t \tag{2.14}$$

$$\bar{l}(\mathbf{v}) = \frac{1}{T}\int_0^T l(\mathbf{v};t)\,\mathrm{d}t. \tag{2.15}$$

Proposition 3. *Problems* (2.11) *and* (2.13) *are equivalent.*

Proof. First, let us show that (2.13) implies (2.11). We suppose by contradiction that (2.13) holds, but (2.11) does not. There exists a function $\mathbf{v}^* \in H^1_{0,\Gamma_D}(\Omega)$ and a positive measure set $D \subset [0,T]$, such that

$$a_\rho(\mathbf{u},\mathbf{v}^*;t) > l(\mathbf{v}^*;t) \quad \forall t \in D. \tag{2.16}$$

Now by taking in (2.13)

$$\mathbf{v} = \mathbf{v}^* \mathbb{1}_D(t) \tag{2.17}$$

we get the contradiction, i.e.

$$\frac{1}{T}\int_0^T a_\rho(\mathbf{u},\mathbf{v};t)\,\mathrm{d}t - \frac{1}{T}\int_0^T l(\mathbf{v};t)\,\mathrm{d}t > 0. \tag{2.18}$$

Now, let us show that (2.11) implies (2.13). Since $H^1_{0,\Gamma_D}(\Omega)$ is separable, it admits a countable basis $\{\mathbf{w}_j\}_{j\in\mathbb{N}}$. Let us consider $\mathbf{v} \in \mathcal{V}$; for almost any $t \in [0,T]$, $\mathbf{v}(t) \in H^1_{0,\Gamma_D}(\Omega(t))$ and it can be extended to a function (that we call $\mathbf{v}(t)$ as well) in $H^1_{0,\Gamma_D}(\Omega)$. We know that the Fourier series of $\mathbf{v}(t)$ converges in $H^1_{0,\Gamma_D}(\Omega)$:

$$\mathbf{v}_N(t) = \sum_{j=0}^{N} c_j(t)\mathbf{w}_j \xrightarrow{H^1_{0,\Gamma_D}(\Omega)} \mathbf{v}(t) \qquad \text{a.e. } t \in [0,T]. \tag{2.19}$$

We apply (2.11) to each $\mathbf{w}_j$, multiply by $c_j(t)$ and sum over j, and we get:

$$a_\rho(\mathbf{u},\mathbf{v}_N;t) = l(\mathbf{v}_N;t) \qquad \text{a.e. } t \in [0,T] \tag{2.20}$$

where the negligible null measure set does not depend on N, since the countable union of null measure sets has null measure. By letting $N \to +\infty$, we get:

$$a_\rho(\mathbf{u},\mathbf{v};t) = l(\mathbf{v};t) \qquad \text{a.e. } t \in [0,T] \tag{2.21}$$

and by integrating between 0 and T, and we get (2.13). □

Remark 1. The integral-in-time formulation (2.13) is more suitable for the development of the theory, while the pointwise-in-time formulation (2.11) will be useful for the numerical approximation, since it allows us to compute the displacement field at each time independently of the other times.

Well-posedness of problem (2.13) can be proved by Lax-Milgram lemma, since it is easy to prove that bilinear form $\bar{a}_\rho(\cdot,\cdot)$ is continuous and coercive on $\mathcal{V}\times\mathcal{V}$ for each $\rho \in \mathcal{U}_{ad}$, and $\bar{l}(\cdot)$ is continuous on $\mathcal{V}$. The bound of the solution is independent of the choice of $\rho \in \mathcal{U}_{ad}$.

2.4 Continuous topology optimization problem

Since we are interested in the whole time dependent printing process, we take as objective functional the mean compliance (where the average is performed both in space and in time):

$$\mathcal{J} = \frac{1}{T}\int_0^T l(\mathbf{u};t)\,\mathrm{d}t = \bar{l}(\mathbf{u}), \tag{2.22}$$

where $\mathbf{u}$ solves the state equation.

Thus, the continuous time dependent topology optimization problem reads as follows

$$\begin{aligned} \min_{\rho\in\mathcal{U}_{ad}} \quad & \bar{l}(\mathbf{u}) \\ \text{s.t.} \quad & \bar{a}_\rho(\mathbf{u},\mathbf{v}) = \bar{l}(\mathbf{v}) \quad \forall \mathbf{v}\in\mathcal{V} \end{aligned} \tag{2.23}$$

or, more explicitly:

$$\begin{aligned} \min_{\rho\in\mathcal{U}_{ad}} \quad & \frac{1}{T}\int_0^T l(\mathbf{u};t)\,\mathrm{d}t \\ \text{s.t.} \quad & \frac{1}{T}\int_0^T\int_{\Omega(t)} E_\rho(\mathbf{x})\mathbf{E}_0\nabla_s\mathbf{u}(t):\nabla_s\mathbf{v}(t)\,\mathrm{d}\mathbf{x}\,\mathrm{d}t = \frac{1}{T}\int_0^T l(\mathbf{v};t)\,\mathrm{d}t \quad \forall\,\mathbf{v}\in\mathcal{V}. \end{aligned} \tag{2.24}$$

We remark that by means of the equivalence between (2.11) and(2.13), the optimization problem (2.24) reduces to a form close to the classical SIMP based minimum compliance problem. Thus, most of the well known solution methods for the classical SIMP problem, such as OC, MMA and CONLIN, can be applied the the evolutionary problem at hand. In particular, in this paper we will consider the OC (Optimality Conditions) method.

2.5 The optimality conditions

In this section we derive optimality conditions for the optimization problem (2.23). The associated Lagrangian function is:

$$\begin{aligned} \mathcal{L} = \bar{l}(\mathbf{u}) - \Big(\bar{a}_\rho(\mathbf{u},\bar{\mathbf{u}}) - \bar{l}(\bar{\mathbf{u}})\Big) + \Lambda\Big(\int_\Omega \rho(\mathbf{x})\,\mathrm{d}\mathbf{x} - C\Big) \\ + \int_\Omega \lambda^+(\mathbf{x})\big(\rho(\mathbf{x})-1\big)\,\mathrm{d}\mathbf{x} + \int_\Omega \lambda^-(\mathbf{x})\big(\rho_{min}-\rho(\mathbf{x})\big)\,\mathrm{d}\mathbf{x} \end{aligned} \tag{2.25}$$

where $\bar{\mathbf{u}}\in\mathcal{V}$ is the Lagrangian multiplier for the state equation (2.13), Λ is the multiplier for the volume constraint (2.8e), $\lambda^+(\mathbf{x})$ for the constraint (2.8b) and $\lambda^-(\mathbf{x})$ for (2.8a). The constraints (2.8c) are (2.8d) are not incorporated in the Lagrangian, but will be considered later by projecting the solution on the space $\mathcal{U}_{ad}$.

By differentiating the Lagrangian function with respect to the state variable $\mathbf{u}$ we get the adjoint equation: find $\bar{\mathbf{u}}$ such that

$$\frac{\partial\mathcal{L}}{\partial\mathbf{u}}(\boldsymbol{\psi}) = \bar{l}(\boldsymbol{\psi}) - \bar{a}_\rho(\boldsymbol{\psi},\bar{\mathbf{u}}) = 0 \qquad \forall\boldsymbol{\psi}\in\mathcal{V}.$$

Thanks to the symmetry properties of elasticity tensor $\mathbf{E}_{ijkl} = \mathbf{E}_{klij}$, the adjoint variable $\bar{\mathbf{u}}$ coincides with state variable $\mathbf{u}$.

Setting $\mathbf{x} = (\mathbf{x}^*, y)$ and differentiating the Lagrangian function with respect to ρ we get:

$$\begin{aligned}\frac{\partial \mathcal{L}}{\partial \rho}(\xi) &= -\frac{1}{T}\int_0^T \int_{\Omega(t)} \frac{\partial E_\rho(\mathbf{x})}{\partial \rho}\xi \mathbf{E}_0 \nabla_s \mathbf{u}(t) : \nabla_s \mathbf{u}(t)\,\mathrm{d}\mathbf{x}\,\mathrm{d}t \\ &\quad + \Lambda \int_\Omega \xi\,\mathrm{d}\mathbf{x} + \int_\Omega \lambda^+(\mathbf{x})\xi\,\mathrm{d}\mathbf{x} - \int_\Omega \lambda^-(\mathbf{x})\xi\,\mathrm{d}\mathbf{x} \\ &= -\frac{1}{T}\int_0^T \int_{\Omega} \frac{\partial E_\rho(\mathbf{x})}{\partial \rho}\xi \mathbf{E}_0 \nabla_s \mathbf{u}(t) : \nabla_s \mathbf{u}(t) \mathbb{1}_{\{y<v_0 t\}}(\mathbf{x})\,\mathrm{d}\mathbf{x}\,\mathrm{d}t \\ &\quad + \int_\Omega \Big[\Lambda + \lambda^+(\mathbf{x}) - \lambda^-(\mathbf{x})\Big]\xi\,\mathrm{d}\mathbf{x} \\ &= \int_\Omega \Big[-\frac{1}{T}\int_{y/v_0}^T \frac{\partial E_\rho(\mathbf{x})}{\partial \rho}\mathbf{E}_0 \nabla_s \mathbf{u}(t) : \nabla_s \mathbf{u}(t)\,\mathrm{d}t + \Lambda + \lambda^+(\mathbf{x}) - \lambda^-(\mathbf{x})\Big]\xi\,\mathrm{d}\mathbf{x} = 0\end{aligned} \tag{2.26}$$

for all $\xi \in L^2(\Omega)$. Hence, the set of optimality conditions reads as follows:

$$\begin{cases} \frac{1}{T}\int_{y/v_0}^T \frac{\partial E_\rho(\mathbf{x})}{\partial \rho}\mathbf{E}_0 \nabla_s \mathbf{u}(t) : \nabla_s \mathbf{u}(t)\,\mathrm{d}t = \Lambda + \lambda^+(\mathbf{x}) - \lambda^-(\mathbf{x}) & \text{a.e. } \mathbf{x} \in \Omega \\ \lambda^+(\mathbf{x}) \geq 0, \qquad \rho(\mathbf{x}) \leq 1, \qquad \lambda^+(\mathbf{x})\big(\rho(\mathbf{x}) - 1\big) = 0 & \text{a.e. } \mathbf{x} \in \Omega \\ \lambda^-(\mathbf{x}) \geq 0, \qquad \rho(\mathbf{x}) \geq \rho_{min}, \qquad \lambda^-(\mathbf{x})\big(\rho_{min} - \rho(\mathbf{x})\big) = 0 & \text{a.e. } \mathbf{x} \in \Omega \\ \Lambda \geq 0, \qquad \int_\Omega \rho(\mathbf{x})\,\mathrm{d}\mathbf{x} \leq C, \qquad \Lambda\Big(\int_\Omega \rho(\mathbf{x})\,\mathrm{d}\mathbf{x} - C\Big) = 0. \end{cases} \tag{2.27}$$

Thus, at a stationary point the following holds:

$$\begin{cases} \Psi(\mathbf{x}) = \Lambda & \text{if } \rho_{min} < \rho(\mathbf{x}) < 1 \\ \Psi(\mathbf{x}) \leq \Lambda & \text{if } \rho(\mathbf{x}) = \rho_{min} \\ \Psi(\mathbf{x}) \geq \Lambda & \text{if } \rho(\mathbf{x}) = 1 \end{cases} \tag{2.28}$$

where we have defined:

$$\begin{aligned}\Psi(\mathbf{x}) &= \frac{1}{T}\int_{y/v_0}^T \frac{\partial E_\rho(\mathbf{x})}{\partial \rho}\mathbf{E}_0 \nabla_s \mathbf{u}(t) : \nabla_s \mathbf{u}(t)\,\mathrm{d}t \\ &= \frac{1}{T}\int_{y/v_0}^T p\rho(\mathbf{x})^{p-1}(1 - E_{min})\mathbf{E}_0 \nabla_s \mathbf{u}(t) : \nabla_s \mathbf{u}(t)\,\mathrm{d}t.\end{aligned} \tag{2.29}$$

2.6 A Continuous fixed point algorithm

Building upon the necessary optimality conditions (2.28) we consider the following classical fixed-point algorithm, where at each iteration the updated density is projected on the space $\mathcal{U}_{ad}$ by setting $\rho = 1$ on Ω_1 and $\rho = \rho_{min}$ on Ω_0:

$$\rho_{K+1} = \begin{cases} \rho_{min} & \text{if } \mathbf{x} \in \Omega_0 \\ 1 & \text{if } \mathbf{x} \in \Omega_1 \\ \max\{(1-\zeta)\rho_K, \rho_{min}\} & \text{if } \rho_K B_K^\eta \leq \max\{(1-\zeta)\rho_K, \rho_{min}\}, \mathbf{x} \notin (\Omega_1 \cup \Omega_0) \\ \min\{(1+\zeta)\rho_K, 1\} & \text{if } \rho_K B_K^\eta \geq \min\{(1+\zeta)\rho_K, 1\}, \mathbf{x} \notin (\Omega_1 \cup \Omega_0) \\ \rho_K B_K^\eta & \text{else} \end{cases} \tag{2.30}$$

where we have defined:

$$B_K(\mathbf{x}) = \frac{\Psi_K(\mathbf{x})}{\Lambda_K} = \\ = \frac{1}{\Lambda_K T}\int_{y/v_0}^{T} p\rho(\mathbf{x})^{p-1}(1-E_{min})\mathbf{E}_0\nabla_s\mathbf{u}(t):\nabla_s\mathbf{u}(t)\,\mathrm{d}t\,. \tag{2.31}$$

The value of the multiplier Λ_K should be chosen in order to satisfy the volume constraint. Since the updated density ρ_{K+1} is a continuous and non increasing function of Λ_K, the value of the multiplier can be computed by resorting, e.g., to a bisection algorithm. The variable ζ is a move limit, and η is a tuning parameter. Both values can be adjust to improve efficiency of the algorithm. Typical values are respectively 0.1 and 0.5. In the actual implementation some filtering procedure must be taken into account to get a well-posed problem.

3 Discretization of the evolutionary topology optimization problem

In this section, we introduce the discretization of the problem (2.11) and we derive the discrete counterpart of the optimization problem (2.23) that will be solved using the OC (Optimality Conditions) method.

3.1 Finite-element space discretization

At the generic time instant t, we consider a computational grid $\mathcal{T}_h(t)$ partitioning the domain $\Omega(t)$ and we denote with $X_h(t)$ the continuous linear finite element space defined on $\mathcal{T}_h(t)$. We introduce the finite element space of functions compatible with the boundary conditions:

$$V_h(t) = \Big\{\mathbf{u}_h \in X_h(t) \quad \text{s.t.} \quad \mathbf{u}_h = 0 \quad \text{on} \quad \Gamma_D\Big\}. \tag{3.1}$$

Let $\{\boldsymbol{\varphi}_j\}_{j=1}^{N_h(t)}$ be a basis of $V_h(t)$, where $N_h(t)$ is the dimension of the space. The space discretization of state equation (2.11) at time t reads:

$$\begin{aligned} \text{find} \quad & \mathbf{u}_h(t) \in V_h(t) \quad \text{s.t.} \\ & a_\rho(\mathbf{u}_h, \mathbf{v}_h; t) = l(\mathbf{v}_h; t) \qquad \forall\, \mathbf{v}_h \in V_h(t). \end{aligned} \tag{3.2}$$

By writing $\mathbf{u}_h(t)$ as linear combination of elements of the basis

$$\mathbf{u}_h(x,t) = \sum_{j=1}^{N_h(t)} u_j(t)\boldsymbol{\varphi}_j, \tag{3.3}$$

we get the Galerkin approximation associated to time t:

$$\mathbf{A}_t\mathbf{U}_t = \mathbf{F}_t \tag{3.4}$$

where

$$[\mathbf{A}_t]_{ij} = a_\rho(\boldsymbol{\varphi}_j, \boldsymbol{\varphi}_i; t), \qquad [\mathbf{U}_t]_j = u_j(t), \qquad [\mathbf{F}_t]_i = l(\boldsymbol{\varphi}_i; t). \tag{3.5}$$

3.2 Discretization in time

We consider a uniform subdivision of the time domain I and we solve the linear system (3.4) at the N time instants $t_n = nT/N, n = 1, \dots, N$. The collection of vectors $\{\mathbf{U}_{t_0}, \dots \mathbf{U}_{t_N}\}$ is the full discretization of the state variable $\mathbf{u}$ over the time interval I. For the sake of simplicity, we consider a structured grid with a vertical discretization such that the grid $\mathcal{T}_h$ on the full space domain Ω can be split into the N horizontal layers $E \times [v_0 t_{n-1}, v_0 t_n]$ for $n = 1, \dots N$. Under this hypothesis, given $\mathcal{T}_h$ and a basis $\{\boldsymbol{\varphi}_j\}_{j \in V}$ of the finite element space V_h defined on $\mathcal{T}_h$, we can recover $V_h(t)$ as the space generated by the subset of $\{\boldsymbol{\varphi}_j\}_{j \in V}$ of functions whose support has non-empty intersection with $\Omega(t_n)$.

When multiple layers ($N > 1$) are used in the computation of the optimal time-averaged compliance, the resulting approach will be referred to as *multi-layer approach*. Otherwise, for $N = 1$ we recover the standard minimal compliance optimization that we will refer to as *single-layer* approach.

3.3 Full discretization

Let K_e be a generic element of the mesh $\mathcal{T}_h$, with index $e \in B$. We denote with B^0 and B^1 the sets of indexes of elements belonging to Ω_0 and Ω_1, respectively. The subset of mesh elements contained in the domain $\Omega(t_n)$ is denoted as $B_n \subset B$. Moreover, let n_e indicate the value of the smallest time step such that the element K_e belongs to $\Omega(t_n)$ and let V_e be the set of indexes of degrees of freedom associated with the element e. Thus the following relations hold:

$$\begin{aligned} &\bigcup_{e \in B} K_e = \Omega, \\ &\bigcup_{e \in B_n} K_e = \Omega(t_n), \\ &e \in B_n \iff n \geq n_e. \end{aligned} \tag{3.6}$$

We remark that the finite element approximation ρ_h of the density is piecewise constant over the triangulation $\mathcal{T}_h$, while the state variable $\mathbf{u}$ is discretized by continuous in space (with basis $\{\boldsymbol{\varphi}_j\}_{j \in V}$) piecewise constant in time finite elements, i.e.

$$\begin{aligned} \rho_h(\mathbf{x}) &= \sum_{e \in B} \rho_e \mathbb{1}_{K_e}(\mathbf{x}), \\ \mathbf{u}_h(\mathbf{x}, t) &= \sum_{n=1}^{N} \sum_{j \in V} u_j^n \boldsymbol{\varphi}_j(\mathbf{x}) \mathbb{1}_{(t_{n-1}, t_n]}(t). \end{aligned} \tag{3.7}$$

We define

$$\begin{aligned} K_{ij}^e &= \int_{K_e} \mathbf{E}_0 \nabla_s \boldsymbol{\varphi}_i : \nabla_s \boldsymbol{\varphi}_j \, \mathrm{d}\mathbf{x}, \\ f_i^e &= \int_{K_e} \rho_0 \mathbf{g} \cdot \boldsymbol{\varphi}_i \, \mathrm{d}\mathbf{x}, \end{aligned} \tag{3.8}$$

and the following SIMP interpolation holds:

$$E(\rho_e) = E_{min} + \rho_e^p (1 - E_{min}). \tag{3.9}$$

Finally, the constraint (2.8e) reads as follows:

$$\sum_{e\in B} |K_e|\rho_e \leq C. \tag{3.10}$$

In view of the above discussion, the discrete counterpart of the minimization problem (2.23) reads as follows:

$$\begin{aligned}
\min_{\{\rho_e\}} \quad & \frac{1}{N}\sum_{n=1}^{N}\sum_{e\in B_n} \mathbb{1}_{B^1}(e)\sum_{i\in V_e} f_i^e u_i^n \\
\text{s.t.} \quad & \frac{1}{N}\sum_{n=1}^{N}\sum_{e\in B_n} E(\rho_e)\sum_{i,j\in V_e} K_{ij}^e u_i^n v_j^n \\
& \qquad = \frac{1}{N}\sum_{n=1}^{N}\sum_{e\in B_n} \mathbb{1}_{B^1}(e)\sum_{i\in V_e} f_i^e v_i^n \quad \forall \{v_i^n\}_{n=1,\dots,N}^{i\in V} \subset \mathbb{R} \\
& \sum_{e\in B} |K_e|\rho_e \leq C \\
& \rho_{min} \leq \rho_e \leq 1 \quad \forall e \in B \\
& \rho_e = \rho_{min} \quad \forall e \in B^0 \\
& \rho_e = 1 \quad \forall e \in B^1.
\end{aligned} \tag{3.11}$$

The Lagrangian function for the discretized problem is defined as follows:

$$\begin{aligned}
\mathcal{L} = & \frac{1}{N}\sum_{n=1}^{N}\sum_{e\in B_n} \mathbb{1}_{B^1}(e)\sum_{i\in V_e} f_i^e u_i^n - \frac{1}{N}\sum_{n=1}^{N}\sum_{e\in B_n}\left(E(\rho_e)\sum_{i,j\in V_e} K_{ij}^e u_i^n u_j^n - \mathbb{1}_{B^1}(e)\sum_{i\in V_e} f_i^e u_i^n\right) \\
& + \Lambda\left(\sum_{e\in B}|K_e|\rho_e - C\right) + \sum_{e\in B}\lambda_e^+\big(\rho_e - 1\big) + \sum_{e\in B}\lambda_e^-\big(\rho_{min} - \rho_e\big).
\end{aligned} \tag{3.12}$$

where Λ is the Lagrangian multiplier for the constraint (2.8e), λ_e^+ for the constraint (2.8b) and λ_e^- for (2.8a). The constraints (2.8c) are (2.8d) are not plugged in the Lagrangian, but will be considered later by projecting the solution on the space $\mathcal{U}_{ad}$ in (3.16).

If we differentiate the Lagrangian with respect to the state variable we get the discrete version of adjoint equation, while deriving with respect to the design variables ρ_e we get:

$$\frac{\partial \mathcal{L}}{\partial \rho_e}(\xi) = \sum_{e\in B}\left[-\frac{1}{N}\sum_{n=n_e}^{N}\left(p\rho_e^{p-1}(1-E_{min})\sum_{i,j\in V_e} K_{ij}^e u_i^n u_j^n\right) + \Lambda|K_e| + \lambda_e^+ - \lambda_e^-\right]\xi. \tag{3.13}$$

By defining

$$\Psi_e = \frac{1}{N|K_e|}\sum_{n=n_e}^{N}\left(p\rho_e^{p-1}(1-E_{min})\sum_{i,j\in V_e} K_{ij}^e u_i^n u_j^n\right) \tag{3.14}$$

we get the optimality conditions for the discretized problem which reads as follows

$$\begin{cases} \Psi_e = \Lambda & \text{if } \rho_{min} < \rho_e < 1 \\ \Psi_e \leq \Lambda & \text{if } \rho_e = \rho_{min} \\ \Psi_e \geq \Lambda & \text{if } \rho_e = 1. \end{cases} \tag{3.15}$$

3.4 A fixed point algorithm for the discrete problem

Based on (3.15), it is possible to derive an Optimality Condition (OC) method that computes a sequence $\{\rho_e^K\}$ approximating ρ_e by resorting to the following fixed-point algorithm: for $K \geq 1$

$$\rho_e^{K+1} = \begin{cases} \rho_{min} & \text{if } e \in B^0 \\ 1 & \text{if } e \in B^1 \\ \max\{(1-\zeta)\rho_e^K, \rho_{min}\} & \text{if } \rho_e^K (Q_e^K)^\eta \leq \max\{(1-\zeta)\rho_e^K, \rho_{min}\}, e \notin (B^1 \cup B^0) \\ \min\{(1+\zeta)\rho_e^K, 1\} & \text{if } \rho_e^K (Q_e^K)^\eta \geq \min\{(1+\zeta)\rho_e^K, 1\}, e \notin (B^1 \cup B^0) \\ \rho_e^K (Q_e^K)^\eta & \text{elsewhere} \end{cases} \tag{3.16}$$

where $Q_e^K = \Psi_e^K / \Lambda^K$.

As in the continuous case, the value of Λ^K can be computed by employing a bisection algorithm. Moreover, some filtering procedure must be taken into account to get a well-posed problem, see e.g. [10].

3.5 Description of the algorithm

In this section, we briefly summarize the different steps required to apply the proposed methodology, from the pre-processing needed to setup the simulation to the actual optimization loop.

1. *Pre-processing*
   - Choose a cylindric reference space domain Ω and identify sub-domains Ω_0 and Ω_1.
   - Subdivide time interval $[0, T]$ into N time steps.
   - Build a spatial mesh $\mathcal{T}_h$ on Ω, fine enough to describe the geometrical details of the sub-domains Ω_0 and Ω_1 and conforming with the horizontal layers at $y = v_0 t_1, \ldots, v_0 t_N$.
   - Build the finite element space V_h with its basis functions.
   - Choose an initial design for the variables ρ_e (for instance a uniform distribution).
2. *Optimization*
   - For each time step t_n, compute the displacement field with the current value of the design variable (see (3.4)).
   - Compute for each mesh element the value of Ψ_e according to (3.14).
   - Compute the current value of Λ_K by bisection.
   - Update the design variables ρ_e as in (3.16).
   - Repeal until a stopping criterion is satisfied.

4 Numerical results

A set of numerical test cases has been carried out to assess the properties of the proposed topology optimization scheme for the design of support structures. The main objective is to show that the proposed multi-layer approach, thanks to the fact that it minimizes the time-average mean compliance during the printing process may lead to different optimal configurations compared to those obtained from a standard single-layer minimal compliance problem for the final shape object. We will also discuss under which conditions on the shape of the object this difference may be more pronounced.

4.1 Test case 1

We first consider a self-supporting structure defined by a tapered beam which is joint to the ground on the left (thinner) extreme and supported by a vertical pillar on the right (thicker) extreme. The structure is depicted in black in Fig 3. The rectangular computational domain expressed in meters is $\Omega = (0, 1) \times (0, 0.5)$ and the prescribed active region $\Omega \setminus \Omega_0 \cup \Omega_1$, where topology optimization procedure can add the supports, is the area below the structure (in light grey in Fig. 3).

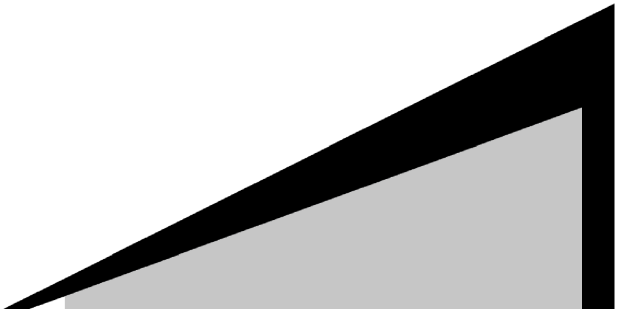

Figure 3: Computational domain for test case 1

The same material, thermoplastic polyurethane with density $\rho_0 = 1.1 \cdot 10^3$ Kg/m^3 and Young's modulus $E = 3 \cdot 10^7$ Pa, has been used for both the object and the supports. However, different materials could be easily considered in the proposed model. The topology optimization has been performed on three mesh resolutions $(50 \times 25, 100 \times 50, 200 \times 100)$ using a sensitivity filter with a fixed (that is, independent of the mesh size) filter size of 0.2. We compare the results obtained using a standard single-layer approach for the final shape object (Fig. 4, left), with the results of the proposed multi-layer approach using 25 time intervals (Fig. 4, right).

The solution of the topology optimization problem is given by the distribution of material in the active region. The main features of the solution, in particular the number of generated supports, are captured even with a coarse grid and, in this respect, the solution is robust as the space resolution is increased. However, position and size of the supports differ for the two approaches. In particular, as shown in Fig. 4, in order to reduce the compliance in the first phases of the printing process, the multi-layer approach generates a set of supports which are shifted on the right and thickened. Indeed, the multi-layer approach in this way should be

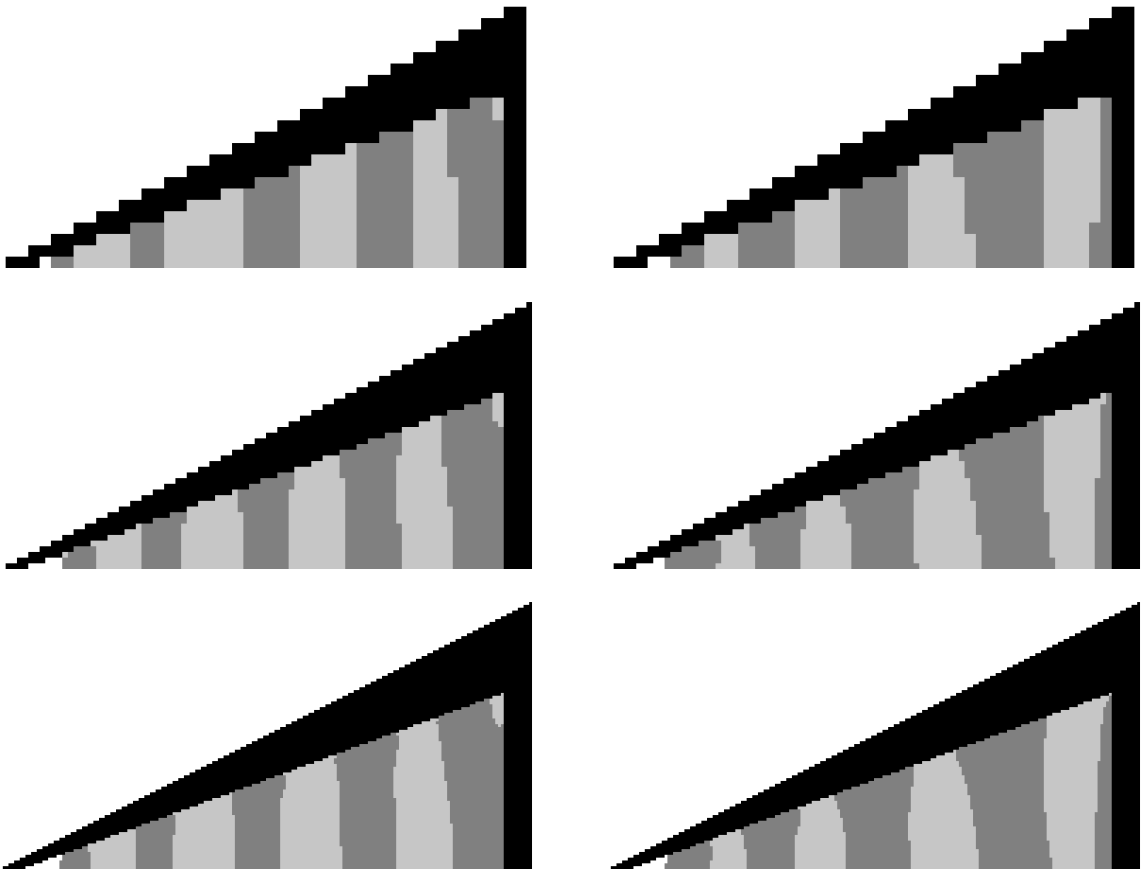

Figure 4: Results of test case 1: single-layer minimization (left), multi-layer minimization (right). Increasing mesh resolution from top to bottom.

able to mitigate the possible transient effect related to the fact that the tapered beam is not self-supporting at the beginning of the process.

The different solutions of the single and multi-layer approaches are obviously due to the different functionals which are minimized. It is interesting to analyze the optimal solutions solution obtained by the two approaches by evaluating the history of the compliance that each solution would display during the printing process. In particular, for both optimal solutions, we have solved a sequence of $M = 50$ linear elasticity problems, for the material distribution restricted in the domain $E \times [0, v_0 t_m]$ with $t_m = mT/M$ for $m = 1, \ldots, M$. The compliance history for both cases is presented in Fig. 5. If, on one hand, the compliance at the final time is lower for the single-layer approach (since in this case the compliance at $t = T$ is exactly the functional that is minimized), on the other hand, the shape obtained using the multi-layer approach guarantees a significant reduction of the compliance over a large portion of the time interval (since, in this case, it is the time integral that is minimized).

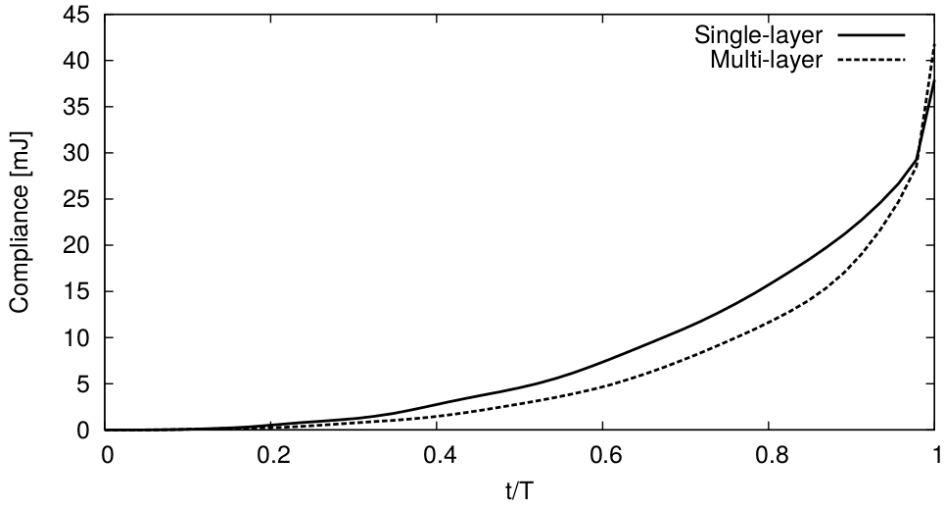

Figure 5: Time-evolution of the compliance for the single-layer solution (solid line) and the multi-layer solution (dashed-line) for test case 1.

4.2 Test case 2

A second test case is proposed, with the aim of highlighting under which conditions the proposed multi-layer approach performs better than the standard one. We consider the two structures, one with a squared profile and the other with a rounded profile, displayed in black in Fig. 6. The structures are fixed on the ground and the domain expressed in meters is $\Omega = (0,1)\times(0,0.25)$, with the prescribed active region (where the support can be added) identified by the grey region below the structure. The material properties and filtering procedure are the same as for test case 1. For both structures we compare the solution obtained with a standard (single-layer) minimum compliance optimization with the one obtained with the proposed multi-layer approach.

Figure 6: Computational domains for test case 2: squared structure (left) and rounded structure (right)

When the squared structure is considered (see Fig. 7), the numerical results obtained with the single and multi-layer approaches are virtually indistinguishable. This is not so surprising since, due to the particular geometry of the squared structure, only the last layers during the evolution can contribute significantly to the mean compliance, since the lateral vertical structure are self-supporting and do not require any additional support. The result is that, in this case, the functionals to be minimized by the two approaches are very similar and so

are the resulting optimal shapes.

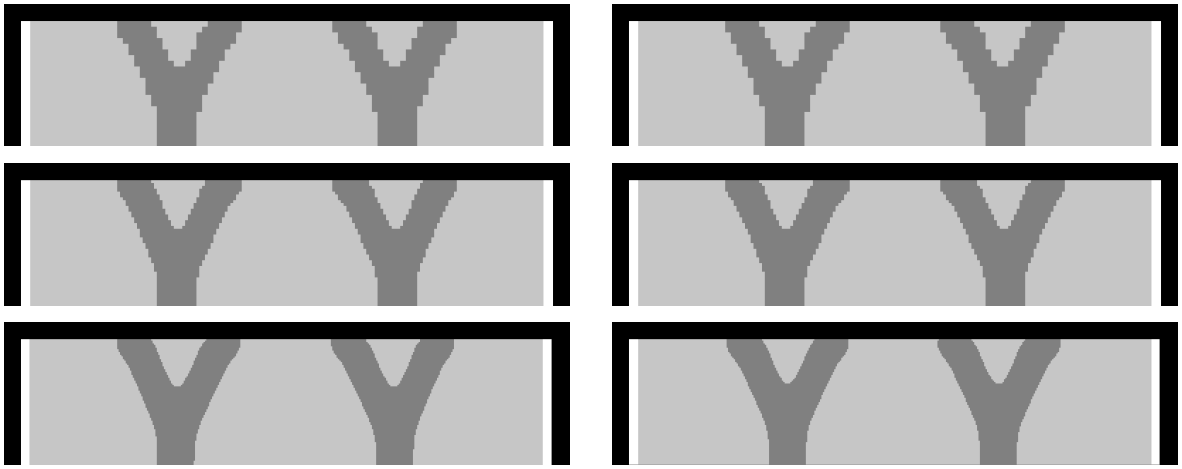

Figure 7: Results of test case 2 (squared structure): single-layer minimization (left), multi-layer minimization (right). Increasing mesh resolution from top to bottom.

Remarkably, when the rounded structure is considered, the two approaches produce very different optimal solutions as displayed in Fig. 8. In this case, the single-layer approach leads to an optimal solution characterized by a double tree-like structure, while for the multi-layer approach a pillar structure is obtained. When the evolutionary nature of the problem is accounted for, the optimization is driven by the fact that at the early stages of the printing process, two overhanging structures need to be supported. This results in an optimal shape obtained with the multi-stage approach characterized by six vertical supporting structures distributed non-uniformly along the domain width.

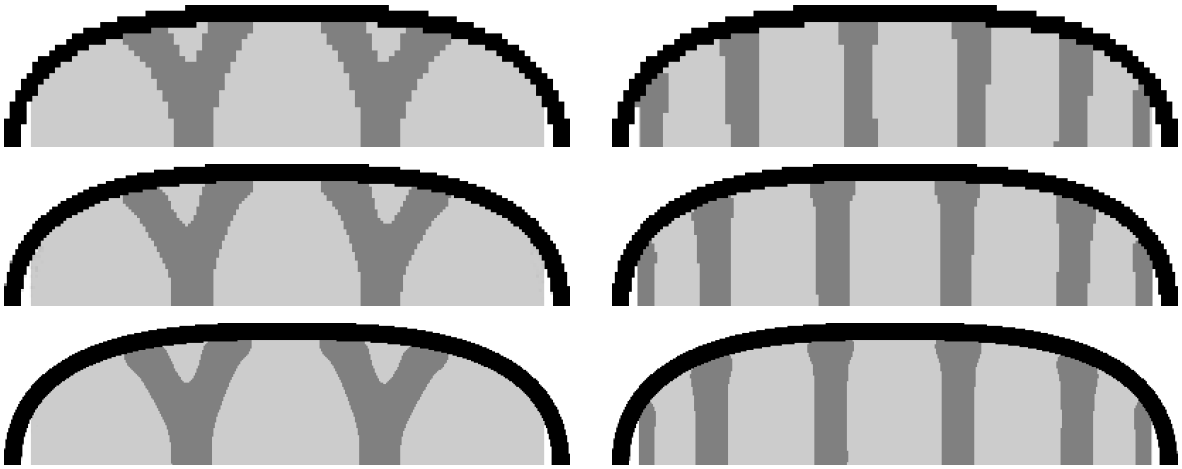

Figure 8: Results of test case 2 (rounded structure): single-layer minimization (left), multi-layer minimization (right). Increasing mesh resolution from top to bottom.

5 Conclusion

We have presented a topology optimization scheme for the optimal placement and design of support structures in problems involving construction stages (such as, e.g., additive manufacturing technologies). The proposed algorithm has been devised for facing the time-dependent nature of this kind of processes, in order to compute the optimal material distribution which minimizes the time-average compliance over a prescribed time interval.

By exploiting the equivalence between the integral-in-time formulation and the pointwise-in-time formulation, it was possible, on one side, to prove the well-posedness of the continuous problem and, on the other side, to derive the optimality conditions for the time-dependent elasticity problem following the standard SIMP approach. This allowed us to define a fixed-point iteration algorithm for the numerical solution of the resulting multi-layer discrete problem, based on the Optimality Condition method.

This proposed numerical scheme, combined with standard filtering techniques, has been used to perform a set of numerical tests. The optimal shapes obtained with the proposed multi-layer approach has been compared with the results of a standard minimal compliance topology optimization algorithm. The results show that the proposed method is able to account for specific evolutionary situations, typical of additive manufacturing processes, such as, for instance, the overhangs appearing in the early stages when printing a self-sustained structure.

6 Acknowledgements

The authors gratefully acknowledge Moxoff s.p.a. for pointing out this interesting topic and for the partial support to this research project.

References

[1] M.P. Bendsoe. Optimal shape design as a material distribution problem. *Structural optimization*, 1(4):193–202, 1989.

[2] M.P. Bendsoe and O. Sigmund. *Topology Optimization*. Springer, 2 edition, 2003.

[3] M. Bruggi, N. Parolini, F. Regazzoni, and M. Verani. Finite element approximation of a time-dependent topology optimization problem. Proceedings of ECCOMAS 2016, 7th European Congress on Computational Methods in Applied Sciences and Engineering, pages 1–13, 2016.

[4] T. Buhl. Simultaneous topology optimization of structure and supports. *Structural and Multidisciplinary Optimization*, 23(5):336–346, 2002.

[5] Joshua D. Deaton and Ramana V. Grandhi. A survey of structural and multidisciplinary continuum topology optimization: Post 2000. *Struct. Multidiscip. Optim.*, 49(1):1–38, January 2014.

[6] C. Fleury. Conlin: An efficient dual optimizer based on convex approximation concepts. *Structural optimization*, 1(2):81–89, 1989.

[7] HH Jang, HA Lee, JY Lee, and GJ Park. Dynamic response topology optimization in the time domain using equivalent static loads. *AIAA journal*, 50(1):226–234, 2012.

[8] C. S. Jog. Topology design of structures subjected to periodic loading. *J. Sound. Vib.*, 3(253):687–709, 2002.

[9] W. Prager and J. E. Taylor. Problems of optimal structural design. *J. Appl. Mech.*, 35(1):102–106, 1968.

[10] O. Sigmund and J. Petersson. Numerical instabilities in topology optimization: A survey on procedures dealing with checkerboards, mesh-dependencies and local minima. *Structural optimization*, 16(1):68–75, 1998.

[11] Ole Sigmund and Kurt Maute. Topology optimization approaches: A comparative review. *Structural and Multidisciplinary Optimization*, 48(6):1031–1055, 2013.

[12] Krister Svanberg. The method of moving asymptotesa new method for structural optimization. *International Journal for Numerical Methods in Engineering*, 24(2):359–373, 1987.

[13] Sajjad Zargham, Thomas Arthur Ward, Rahizar Ramli, and Irfan Anjum Badruddin. Topology optimization: a review for structural designs under vibration problems. *Structural and Multidisciplinary Optimization*, 53(6):1157–1177, 2016.

[14] Tomás Zegard and Glaucio H. Paulino. Bridging topology optimization and additive manufacturing. *Structural and Multidisciplinary Optimization*, 53(1):175–192, 2016.

[15] JH Zhu and WH Zhang. Integrated layout design of supports and structures. *Computer Methods in Applied Mechanics and Engineering*, 199(9):557–569, 2010.

MOX Technical Reports, last issues

Dipartimento di Matematica
Politecnico di Milano, Via Bonardi 9 - 20133 Milano (Italy)

13/2017 Gigante, G.; Vergara, C.
Optimized Schwarz Methods for circular flat interfaces and geometric heterogeneous coupled problems

09/2017 Antonietti, P.F.; Ferroni, A.; Mazzieri, I.; Paolucci, R.; Quarteroni, A.; Smerzini, C.; Stupazzin
Numerical modeling of seismic waves by Discontinuous Spectral Element methods

10/2017 Pini, A.; Stamm, A.; Vantini, S.
Hotelling's T^2 in separable Hilbert spaces

11/2017 Ferro, N.; Micheletti, S.; Perotto, S.
Anisotropic Mesh Adaptation for Crack Propagation Induced by a Thermal Shock

12/2017 Gasperoni, F.; Ieva, F.; Barbati, G.; Scagnetto, A.; Iorio, A.; Sinagra, G.; Di Lenarda, A.
Multi state modelling of heart failure care path: a population-based investigation from Italy

08/2017 Ambrosi, D.; Beloussov, L.V.; Ciarletta, P.
Mechanobiology and morphogenesis in living matter: a survey

06/2017 Ekin, T.; Ieva, F.; Ruggeri, F.; Soyer, R.
On the Use of the Concentration Function in Medical Fraud Assessment

07/2017 Cabassi A.; Pigoli D.; Secchi P.; Carter P.A.
Permutation tests for the equality of covariance operators of functional data with applications to evolutionary biology

05/2017 Menafoglio, A.; Hron, K.; Filzmoser, P.
Logratio approach to distributional modeling

04/2017 Dede', L; Garcke, H.; Lam K.F.
A Hele-Shaw-Cahn-Hilliard model for incompressible two-phase flows with different densities